Guided Proofreading of Automatic Segmentations in Connectomics

Daniel Haehn[1] Verena Kaynig[1,2] James Tompkin[1] Jeff W. Lichtman[2] Hanspeter Pfister[1]

[1]Harvard Paulson School of Engineering and Applied Sciences
[2]Harvard Center for Brain Science
Cambridge, MA 02138, USA
haehn@seas.harvard.edu

Abstract

Automatic cell image segmentation methods in connectomics produce split *and* merge *errors, which require correction through proofreading. To aid error correction, we develop two classifiers to recommend candidate errors and their corrections to the user. These classifiers are informed by training a convolutional neural network with known errors in automatic segmentations against expert-labeled ground truth. Our classifier detects potentially-erroneous regions by considering a large context region around a segmentation boundary. With recommendations, proofreading of mouse cortex electron microscopy image segmentations can reduce variation of information scores on two different datasets from 0.48 to 0.40, which is an improvement on both pure automatic and pure manual proofreading.*

1. Introduction

In connectomics, neuroanatomists annotate neurons and their connectivity within 3D volumes to gain insight into the functional structure of the brain. Rapid progress in automatic sample preparation and electron microscopy (EM) acquisition techniques has made it possible to image large volumes of brain tissue at $\approx 6\,nm$ per pixel to identify cells, synapses, and vesicles. For $25\,nm$ thick sections, a $1\,mm^3$ volume of brain contains 10^{15} voxels, or 1 petabyte of data. With so much data, manual annotation is infeasible, and automatic annotation methods are needed [14, 22, 25, 19].

Automatic annotation by segmentation and classification of brain tissue is challenging [1]. The state of the art uses supervised learning with convolutional neural networks [11], or potentially even unsupervised learning [9]. Typically, cell membranes are detected in 2D images, and the resulting region segmentation is grouped into geometrically-consistent cells across registered sections. Cells may also be segmented across registered sections in 3D directly. Using dynamic programming techniques [23] and a GPU cluster, these classifiers can segment ≈ 1 terabyte of data per hour [17], which is sufficient to keep up with the 2D data capture process on state-of-the-art electron microscopes (though 3D registration is still an expensive offline operation).

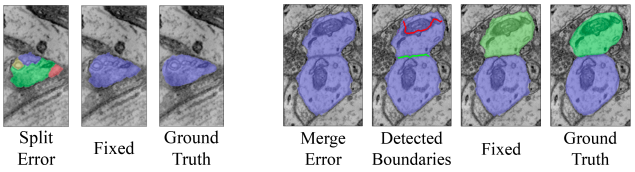

Figure 1: Split and merge error examples, their corrections, and their ground truths.

All automatic methods make errors, and we are left with large data which needs *proofreading* by humans. This crucial task serves two purposes: 1) to correct errors in the segmentation, and 2) to provide a large body of labeled data to train better automatic segmentation methods. Recent proofreading tools provide intuitive user interfaces to browse segmentation data in 2D and 3D and to identify and manually correct errors [31, 15, 20, 13, 16, 32]. Many kinds of errors exist, such as inaccurate boundaries, but the most common are *split errors*, where a single cell is labeled as two, and *merge errors*, where two cells are labeled as one (Fig. 1). With user interaction, split errors can be joined, and the missing boundary in a merge error can be defined with manually-seeded watersheds [13]. However, even with semi-automatic correction tools, the visual inspection to find errors in the first place takes the majority of the time.

Our goal is to add automatic detection of split and merge errors to proofreading tools. Instead of the user visually inspecting the whole data volume carefully to spot errors, we design automatic classifiers that detect split and merge errors in 2D segmentations. Then, a proofreading tool can recommend regions with a high probability of an error to the user, and suggest corrections to accept or reject. We call

this process *Guided Proofreading*.

Given a membrane segmentation from a fast automatic method, our classifiers operate on the boundaries of whole cell regions. Compared to techniques that must analyze every input pixel, we reduce the data analysis to the boundaries only. This allows us to employ wider convolutional neural networks that take regional context and multiple input channels into account. One reason to classify errors on 2D images lies with the cost of 3D registration. This is often slow as it requires non-linear image alignment [4, 30]. However, typically segmentation results are local decisions at the cell level. In this case, 3D reconstruction is unnecessary and, instead of waiting for the 3D output, proofreading can start immediately to maximize error correction before cell grouping occurs across sections.

We quantitatively validate our approach with variation of information (VI) versus ground truth expert segmentations. While unintuitive, VI is a common metric to evaluate region segmentation performance [24]. We compare our approach to an existing proofreading tool that provides only manual error correction [13]. With a simulated user, our automatic error suggestions and corrections decrease VI from 0.4764 to 0.3996, which is in contrast to pure manual or pure automatic methods that can both *increase* VI. On a second larger dataset, our method decreases VI from 0.4847 to 0.3946. As a consequence, we are able to provide tools to proofread segmentations more efficiently, and so better tackle large volumes of connectomics imagery.

2. Related Work

Automatic Segmentation Multi-terabyte EM brain volumes require automatic segmentation [14, 22, 24, 25], but can be hard to classify due to ambiguous intercellular space: the 2013 IEEE ISBI neurites 3D segmentation challenge [1] showed that existing algorithms which learn from expert-segmented training data still exhibit high error rates.

NeuroProof [2] tries to decrease error rates with interactive learning of agglomeration of over-segmentations of images, based on a random forest classifier. Vazquez-Reina et al. [33] propose automatic 3D segmentation by taking whole EM volumes into account rather than a per section approach, then solving a fusion problem with a global context. Kaynig et al. [18] propose a random forest classifier coupled with an anisotropic smoothing prior in a conditional random field framework with 3D segment fusion. It is also possible to learn segmentation classification features directly from images with CNNs. Ronneberger et al. [28] use a contracting/expanding CNN path architecture to enable precise boundary localization with small amounts of training data. Lee et al. [21] recursively train very deep networks with 2D and 3D filters to detect boundaries.

These approaches make good progress; however, in general, proofreading is required to improve them through generating more ground-truth segmentations.

Arganda-Carreras et al. [7] posed the ISBI 2D EM segmentation challenge in 2012, where a 30-image corpus of fly cell 'in/out' labels was used to train boundary detection. However, mouse brain EM data is more difficult than the ISBI 2012 challenge, as it contains significant intercellular space which is hard to classify.

Bogovic et al. [9] learn 3D features, and show even that unsupervised learning can produce better features than hand-designs. We extend the features reported by Bogovic et al. but limit the classification to 2D images rather than 3D. In this case, reconstruction is unnecessary and, instead of waiting for the alignment of the 3D output, proofreading can start immediately to maximize throughput.

Collaborative Interactive Segmentation Recent works attack the problem of massive volume segmentation through crowd-sourcing[29, 6]. EyeWire [3] asks novice users to participate in a segmentation game with neuronal structures using a semi-automatic algorithm. D2P [12] uses a micro-labor workforce approach where local boolean decisions are combined to produce a consensus segmentation. In general, our goal is to correct the output of a segmentation which is thought to be good; hence, our tool would be used after learning a segmentation model to direct user attention to correct likely erroneous areas.

Proofreading Tools Janelia Farms identified the need for proofreading methods in 2010 [10]. The authors introduced Raveler [15], a software targeting expert users by offering many parameters for tweaking the proofreading process at the cost of a higher complexity. Raveler also includes a simple 3D renderer to validate corrections across slices.

The editing bottleneck for existing imperfect automatic segmentations was further specified by Peng et al. [26]. The authors developed software which supports three-dimensional proofreading and envision crowdsourcing to tackle large amounts of data.

EyeWire [3] exists since 2012 and is a popular online platform where users annotate retinal neurons. The platform is set up as an online game and participants earn virtual rewards for merging superpixels to reconstruct the data.

To simplify proofreading of small volumes, Sicat et al. proposed a graph abstraction method to guide users to problematic regions indicating the need for corrections [31].

Later, Plaza suggested a focused proofreading approach using heuristics to concentrate on certain regions of image data [27]. The main driver of his approach is the size of the segment — ignoring very small regions. By doing so, Plaza limits user decisions to yes/no questions and suggests crowdsourcing as a potential platform for proofreading.

In 2014, Haehn et al. developed two proofreading tools: Mojo and Dojo. Mojo provides a simple scribble interface

for error correction, and Dojo extends this for distributed proofreading via a minimalistic web-based user interface. The authors defined requirements for general proofreading tools, and then evaluated the accuracy and speed of Raveler, Mojo, and Dojo through a quantitative user study (Sec. 3 and 4) [13]. Al-Awami et al. integrated Dojo into the Neuroblocks proofreading management system [5], which tracks and visualizes progress among multiple users.

In 2015, Karimov et al. proposed a guided volume editing approach using histogram dissimilarity [16]. Measuring differences in histogram distributions helps to find potential errors and to suggest possible corrections. These promising results on Computed-Tomography Angiography datasets are targeted towards expert users.

Recently, Uzunbas et al. showed that potential labeling errors can be found by considering the merge tree of an automatic segmentation method [32]. The authors track uncertainty through automatic labeling and then present potential regions for proofreading. This requires access to the segmentation merge tree, which is not always available.

However, none of these methods leverage machine learning to enhance the proofreading performance.

3. Method

We build a split error classifier using a convolutional neural network (CNN) to check the boundaries of an existing automatic segmentation. For each boundary, the CNN provides a probability that points sampled along the boundary have caused a split error. For each boundary, we sample up to 10 decision points, where the decision points are spread evenly over the boundary length, given that their context windows do not overlap. These probabilities are then weighted by the length of the boundary within the context over the total boundary length, and averaged. A greedy algorithm then merges neighboring regions sequentially, starting with the highest probability score. Following each merge, neighboring boundaries are re-evaluated for split errors. Correcting a split error is as simple as merging the two bordering labels.

Identification and correction of merge errors is more challenging, because we must look inside segmentation regions for missing or incomplete boundaries and then propose the correct boundary. However, we can reuse the same trained CNN for this task. For each segmentation label, we generate 30 potential boundaries through the region by placing watershed seed points at opposite sides of the label boundary and generating the corresponding split. Then, we check to see whether any potential edge is classified as a split error. If the CNN detects a boundary with a very low split error score, then the boundary should have been in the segmentation and the region is a candidate for a merge error.

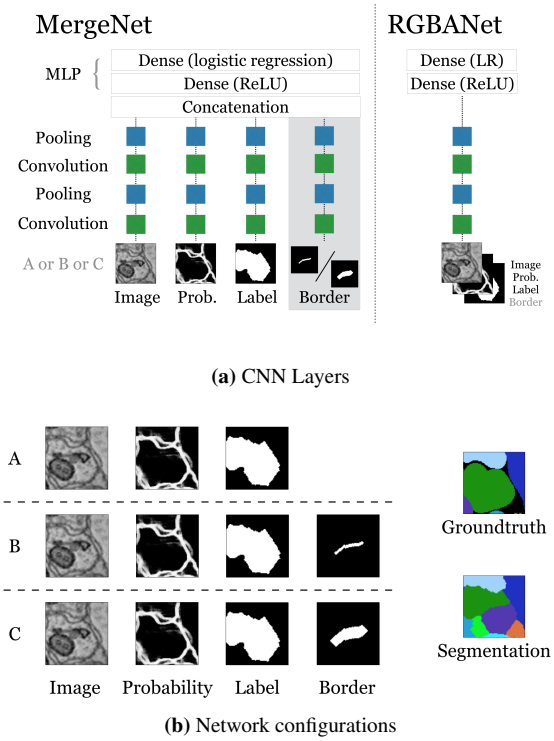

(a) CNN Layers

(b) Network configurations

Figure 2: (a) Our network architecture with up to four input channels, each with two convolutional and two pooling layers. MergeNet includes four separate input channels and RGBANet uses a 4-channel input. (b) We trained three different network configurations with three and four inputs: A) image, boundary map probability, and merged binary mask; B) A configuration extended with a small border mask, to focus on the specific boundary in question; C) A configuration extended with a large border mask.

3.1. Convolutional Neural Network Design

To train a CNN for split error detection, we take multiple channels of boundary context information into consideration for the decision making process. We pass multiple inputs into the CNN windowed around a particular decision pixel: the input grayscale image patch, the corresponding boundary probability map patch, and two corresponding binary mask patches for the segmented regions at either side of the boundary. Following Bogovic et al. [9], these two masks can be combined into a single mask with comparable performance (configuration A, Fig. 2b). The network then leverages these multiple input patches to identify and correct errors made by the previous membrane detection network and automatic segmentation pipeline.

One way to combine these inputs is to treat them as a 4-channel input (‘*RGBANet*’), so that alignment between the input image and the segmentation masks is not lost throughout the convolutions. However, training a boundary-classifying network can be difficult due to rigid ground-

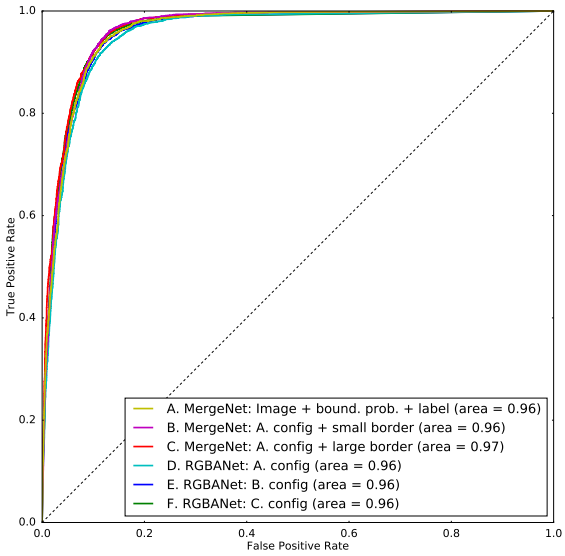

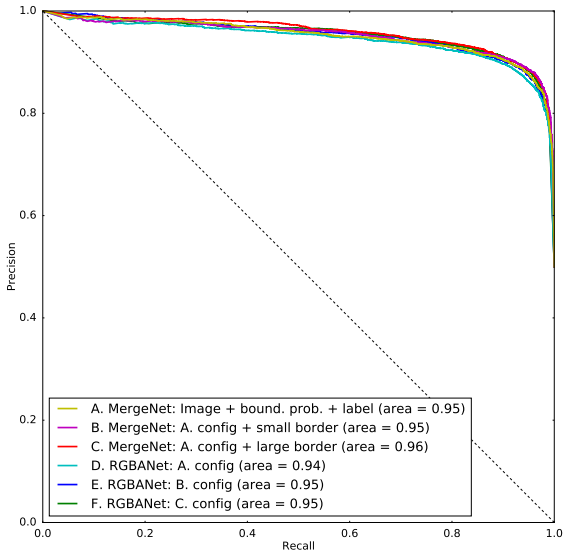

	Network	Validation loss	Test acc.	Prec./Recall	F1 Score
A.	MergeNet: Image + boundary prob. + seg. label	0.073	0.906	0.906/0.906	0.907
B.	MergeNet: A config. + small border overlap ($d = 1$)	0.070	0.911	0.911/0.911	0.912
C.	MergeNet: A config. + large border overlap ($d = 5$)	0.070	0.908	0.908/0.908	0.909
D.	RGBANet: A config.	0.058	0.895	0.895/0.895	0.894
E.	RGBANet: B config.	0.054	0.907	0.907/0.907	0.908
F.	RGBANet: C config.	0.058	0.905	0.905/0.905	0.904

Figure 3: Network design training evaluation. Adding an extra channel containing a binary mask of just the border slightly increases performance in both network configurations. Due to slightly larger areas under the curves for both receiver operating characteristic and precision/recall, we choose configuration MergeNet C to evaluate VI against human performance.

truth segmentations, which often differ substantially from automatic segmentation regions in ambiguous extra-cellular space. To cope with this variation, our network is based on multiple separate input channels ('*MergeNet*', Fig. 2a). Each of the input patches is connected individually to a 2-layer network, with each layer consisting of convolutional and pooling layers. The output of these networks is then combined by a fully-connected multi-layer perceptron (MLP) with one hidden layer and a two-class logistic regression output layer. The intuition for this multiple input channel approach is that we want to allow variation in the input and masks independently to accommodate potential error, and then for the hidden layers to discover appropriate combinations of the relevant features learned separately for the different input channels.

To better direct both networks to train on the true boundary edge, which in many cases is missing from the boundary probability map and hence is the cause of merge errors, we additionally pass as input a second binary mask. This mask contains the true boundary edge (configuration B, Fig. 2b). To consider slight edge ambiguities, we also test a version of this network where the true boundary mask has been dilated by 5 pixels (configuration C).

3.2. Training

To train the network, we use the blue 3-cylinder mouse cortex volume of Kasthuri et al. [17] ($2048 \times 2048 \times 300$ voxels). The tissue is dense mammalian neuropil from layers 4 and 5 of the S1 primary somatosensory cortex of a healthy mouse. The resolution of our dataset is $3\,nm$ per pixel, and the section thickness is $30\,nm$. A manually-labeled expert segmentation is available as ground truth for the entire dataset. We use the first 250 sections of the data for training and validation (split 0.25) and the last 50 for testing. To generate training data, we identify correct regions and split errors in the automatic segmentation by intersection with ground truth regions. From these regions, we sample 266,088 correct regions and 266,088 split error

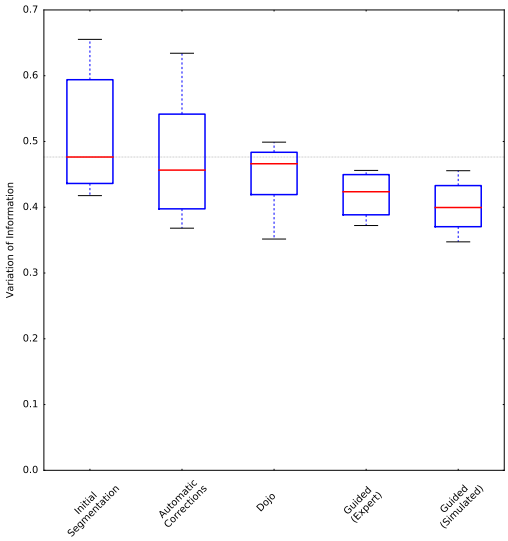

(a) Interactive (Dojo) vs. Guided Proofreading

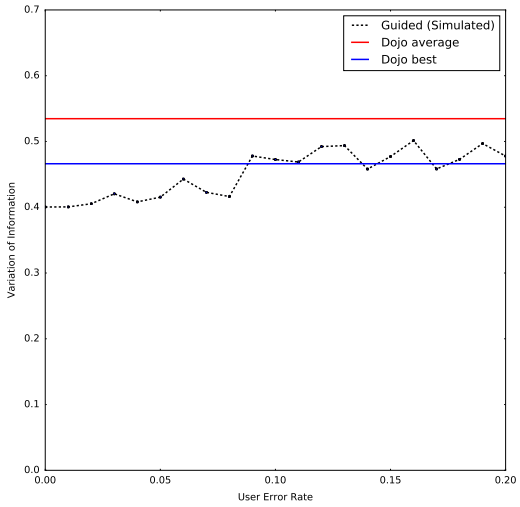

(b) Simulated User Error Rate

Figure 4: (a) We compare distributions of VI measures across 10 sections for five cases: the initial automatic segmentation, a fully-automatic correction of recommended errors based on a threshold of acceptance, the best user in the Haehn et al. experiment with Dojo, two experts using our system, and our simulated user. Lower scores are better. (b) We test our simulated user with different error rates and compare against the best user as well as the average user performance in Dojo.

patches. We define patches of size 75×75 to cover approximately 80% of all boundaries in our segmentation output.

We train our networks using the following parameters: learning rate $lr = 0.03$ (iteratively decreasing until $lr = 0.00001$), momentum $m = 0.9$ (iteratively increasing until $m = 0.999$), filter size $fs = 13 \times 13$, and number of filters $fn = 16$ for MergeNet ($fn_1 = 64, fn_2 = 48$ for RGBANet). This results in approximately 1.5 million parameters for all network configurations. For regularization, we use dropout layers after each pooling layer with $p = 0.2$. We assume that the training has converged if the validation loss does not decrease for 50 epochs. The network is specified using the deep learning libraries Lasagne and Theano [8], and trained on a Tesla K40m graphics card.

Figure 3 presents validation loss function scores (cross validation), test accuracy percentages, precision/recall scores, and F1 scores. We also show receiver operating characteristics and precision/recall curves. We observe a slightly increased performance for networks using the MergeNet configuration. From this, we select configuration MergeNet C to evaluate against human performance in a VI improvement experiment.

4. Evaluation

We evaluate our split and merge error detection and correction recommendation in the context of interactive proofreading tools: to direct users to regions with a high probability of error and to suggest corrections (Fig. 4). For comparison, we take publicly available mouse cortex data of the same kind as our training data. We perform two experiments: first, we compare our approach with previously reported proofreading results using real-world measurements; second, we evaluate guided proofreading in a simulated context with a much larger dataset.

4.1. Comparison Study

For our first experiment, our dataset is part of the ISBI 2013 challenge training dataset ($1024 \times 1024 \times 100$ voxels) which was acquired using a serial section scanning electron microscope (ssSEM) with a resolution of $6 \times 6 \times 30\,nm$ per voxel. We use the available manually-labeled ground truth to score our approach using the variation of information (VI) metric, which is closely related to mutual information. VI is a measure of the distance between two clusterings, where lower VI numbers are better. Since our classifiers are trained on 2D image slices, we perform all evaluations on slices rather than 3D volumes.

Guided proofreading. Recently, Haehn et al. discussed requirements for interactive proofreading and evaluated three different connectomics tools in a study with naive users [13]. This study asked users to spend 30 minutes

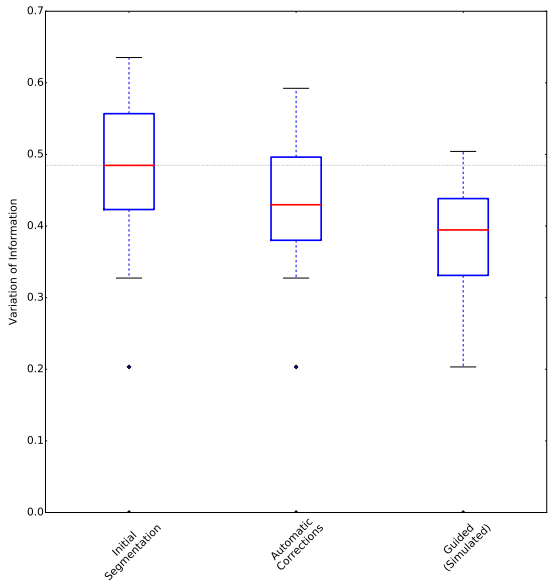

(a) Guided Proofreading Results

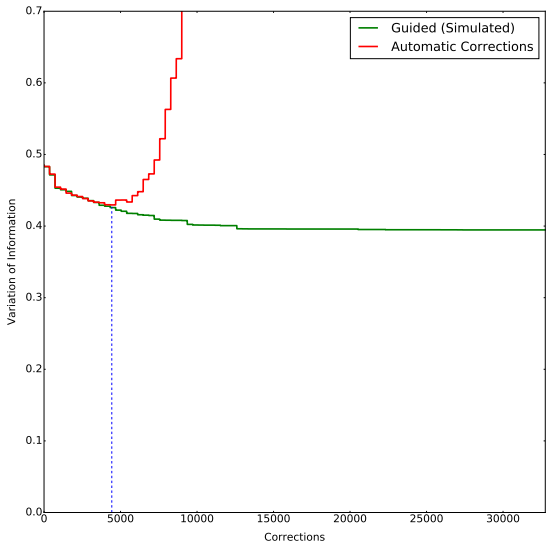

(b) Variation of Information per Correction

Figure 5: Results of our simulated experiment on a larger dataset ($2048 \times 2048 \times 50$ voxels). Lower VI scores are better. (a) The initial segmentation is reduced by both fully-automatic correction (probability threshold $p_t = 0.95$) and our simulated user. (b) We compare the change in VI measure for each individual correction running automatically and user-driven. The dashed blue line indicates the moment p_t is reached. Guided proofreading is able to reduce VI beyond this threshold.

proofreading split and merge errors with the different tools to improve upon the automatic segmentation. The best performing tool in their evaluation was Dojo. We use their findings and their user-generated proofreading result data, which they kindly provided, as a baseline for the evaluation of our method. Haehn et al. performed their user study on the most representative sub-volume ($400 \times 400 \times 10$ voxels) in terms of object size distribution. For comparison, we use the same data and time constraints. We asked two experts to perform the proofreading task using our system (Fig. 6).

In addition, we simulate a user to provide insight into achievable performance. We assume that all classification has been computed ahead of time, and that the user is presented with a stream of error corrections to assess. The assessment is simulated by comparing the VI before and after each recommendation, and only accepting corrections when VI reduces. We test this across different user error rates (Fig. 4). In Haehn et al., the proofreading time was 30 minutes, in which human participants performed 59 corrections on average ($\approx$ 30 seconds per correction). In our scenario, and unlike in Haehn et al., users do not need to visually find errors and manually correct them. From real-world user performance, we observed an average decision time of 3.2 seconds. Thus, for our simulated user, we assume each correction assessment takes 5 seconds (360 assessments in 30 minutes). Split errors are likely to take less time than this; however, merge errors are harder to assess, as the user must select between the top 5 candidate boundaries. Since the performance of Haehn et al.'s human participants showed large variation (average VI improvement: -0.0582), we present the best performing Dojo user (VI improvement: 0.0102) as our baseline. The average VI improvement of two experts using our new system is 0.0528. For our simulated user, the VI improvement is 0.0768 (Fig. 4). In total, our classifier predicted 18 merge and 842 split errors.

Random recommendations. We test a classifier with random performance in comparison to our learned CNN. For split errors, the simulated user is presented with randomly picked boundaries, which they can accept or reject. For merge errors, the simulated user is presented with 5 randomly selected boundaries from the interior of the segmented region. Around 80% of all presented regions did not need to be corrected. Hence, the median VI did not decrease much (VI improvement: 0.0011). The significantly worse performance of this approach demonstrates that our network is informative to the user.

Automatic correction. As a comparison, we also perform automatic correction. During training, we define a probability threshold $p_t = 0.95$ for automatic split correction based on CNN probability from the test set. Then, for automatic correction, we apply both classifiers to produce lists of split and merge errors sorted by confidence. First, we correct merge errors with $\max(1-p)$, followed by split error correction using p_t. The total time for correcting all errors was 17 minutes on a 3.2 GHz Quad-core Intel Xeon with an NVIDIA GeForce Titan (merge error correction 15min, split error correction 2min). The median VI improvement vs. ground truth was 0.02 (Fig. 4). This is not surprising, as the problem is very challenging, and this motivates the need for human-in-the-loop proofreading tools.

4.2. Simulated Experiment

For our second experiment, we proofread 50 slices of the blue 3-cylinder cortex volume of Kasthuri et al. [17]. The data was not seen by the network before and includes 2048 x 2048 x 50 voxels with a total number of 33,076 labeled objects. Since interactive proofreading of such a large dataset would consume a significant amount of time, we restrict our experiment to a simulated user and to automatic corrections. Similar to our comparison study (Sec. 4.1), the simulated user assesses a stream of errors by comparing VI before and after each performed correction. As before, corrections are only accepted when VI reduces. In contrast to our time limit in the comparison study, the simulated user proofreads until all objects in the volume were assessed. For automatic corrections, we use our defined probability threshold $p_t = 0.95$. Based on a time budget of 5 seconds per correction, the proofreading process for a real user would in theory take over 45 hours for this dataset. The total time for automatically correcting all errors was $\approx$ 6 hours on a 3.2 GHz Quad-core Intel Xeon with an NVIDIA Geforce Titan. The total time for the simulated user including the VI calculations after each assessment was $\approx$ 10 hours. Both approaches significantly reduce the VI in comparison to the initial segmentation by 0.0901 for the simulated user and by 0.0549 automatically (Fig. 5).

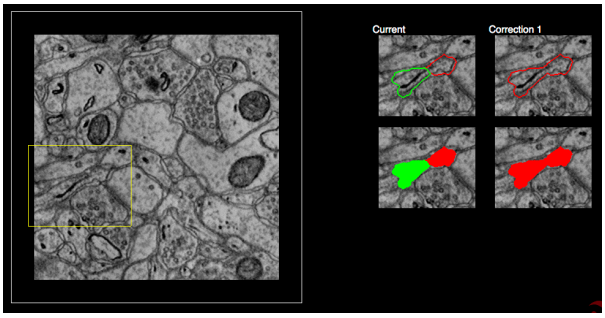

(a) Split error

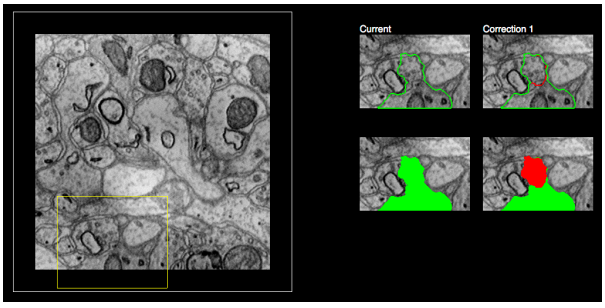

(b) Merge error

Figure 6: Our web-based user interface includes a slice overview with the relevant area highlighted in yellow. The interface shows (a) a split error with a suggested correction as well as (b) a merge error with correction. The user selects whether to accept a correction or to discard it.

5. Application

In our experiments, we observed the best performance using a combination of user guidance and our trained network. In contrast to fully interactive proofreading tools like Dojo, Mojo, and Raveler, our system requires only minimal user input. We distinguish between merge and split errors and provide a very simple user interface to correct them (Fig. 6). The system shows only one potential error in the interface: either a potential false merge or split. In the case of merge errors, the user sees the five highest-scoring possible boundaries as overlays on the corresponding grayscale image, and can also draw a new boundary interactively. The user then chooses one of the suggestions, draws a boundary, or marks the cell as correct. For split errors, the system shows the grayscale image and a possible border, and the user marks whether the cell is correct. Our Dojo user study experiment baseline was limited to 30 minutes, and participants performed 59 corrections in average ($\approx$ 30 seconds per correction). Our experiments suggest that even non-experts can perform a correction using our system in < 5 seconds, resulting in increased proofreading throughput.

6. Discussion and Conclusion

Automatic cell boundary segmentation is difficult, and trying to improve such segmentations automatically as a post-process through split and error correction is, in principle, no different than trying to improve the underlying cell boundary segmentation. This is shown by the approximately equivalent VI distributions of the initial segmentation and our automatic segmentation correction (Fig. 4). Due to the task difficulty, manual proofreading of connectomics segmentations is necessary, but it is time consuming and error prone, as can be seen from the Dojo human trials: on average, participants made the segmentations worse. However, there is value in being able to recommend to users

possible regions for correction, as the time cost of proofreading is dominated by the visual search for errors.

We have addressed this problem through training a CNN to detect ambiguous regions from labeled data—in effect, (re-)learning a confidence measure on boundaries. This allows us to identify split and merge errors, and also to recommend their corrections, which is an improvement over existing systems which just provide semi-automatic merge error correction. Our experiments have shown that guided proofreading has the potential to reduce VI over existing interactive proofreading tools. This helps reduce the proofreading bottleneck in the analysis of large connectomics datasets. To encourage testing of our proposed architecture on more data, we provide the trained networks and classifier code as free and open source software at (link omitted for review).

References

[1] IEEE ISBI challenge: SNEMI3D - 3D segmentation of neurites in EM images. http://brainiac2.mit.edu/SNEMI3D, 2013. Accessed on 31/03/2016. 1, 2

[2] Neuroproof: Flyem tool, hhmi / janelia farm research campus. https://github.com/janelia-flyem/NeuroProof, 2013. Accessed on 03/15/2106. 2

[3] Eyewire. http://eyewire.org/, 2014. Accessed on 31/03/2014. 2

[4] A. Akselrod-Ballin, D. Bock, R. Reid, and S. Warfield. Improved registration for large electron microscopy images. In *IEEE Int. Symp. Biomedical Imaging (ISBI)*, 2009. 2

[5] A. K. Al-Awami, J. Beyer, D. Haehn, N. Kasthuri, J. W. Lichtman, H. Pfister, and M. Hadwiger. Neuroblocks - visual tracking of segmentation and proofreading for large connectomics projects. *IEEE Transactions on Visualization and Computer Graphics*, 22(1):738–746, Jan 2016. 3

[6] J. Anderson, S. Mohammed, B. Grimm, B. Jones, P. Koshevoy, T. Tasdizen, R. Whitaker, and R. Marc. The Viking Viewer for connectomics: Scalable multi-user annotation and summarization of large volume data sets. *Journal of Microscopy*, 241(1):13–28, 2011. 2

[7] I. Arganda-Carreras, S. C. Turaga, D. R. Berger, D. Ciresan, A. Giusti, L. M. Gambardella, J. Schmidhuber, D. Laptev, S. Dwivedi, J. M. Buhmann, T. Liu, M. Seyedhosseini, T. Tasdizen, L. Kamentsky, R. Burget, V. Uher, X. Tan, C. Sun, T. Pham, E. Bas, M. G. Uzunbas, A. Cardona, J. Schindelin, and H. S. Seung. Crowdsourcing the creation of image segmentation algorithms for connectomics. *Frontiers in Neuroanatomy*, 9(142), 2015. 2

[8] F. Bastien, P. Lamblin, R. Pascanu, J. Bergstra, I. J. Goodfellow, A. Bergeron, N. Bouchard, and Y. Bengio. Theano: new features and speed improvements. Deep Learning and Unsupervised Feature Learning NIPS 2012 Workshop, 2012. 5

[9] J. A. Bogovic, G. B. Huang, and V. Jain. Learned versus hand-designed feature representations for 3d agglomeration. *CoRR*, abs/1312.6159, 2013. 1, 2, 3

[10] D. B. Chklovskii, S. Vitaladevuni, and L. K. Scheffer. Semi-automated reconstruction of neural circuits using electron microscopy. *Current Opinion in Neurobiology*, 20(5):667 – 675, 2010. Neuronal and glial cell biology New technologies. 2

[11] D. C. Ciresan, A. Giusti, L. M. Gambardella, and J. Schmidhuber. Deep neural networks segment neuronal membranes in electron microscopy images. In *NIPS*, 2012. 1

[12] R. J. Giuly, K.-Y. Kim, and M. H. Ellisman. DP2: Distributed 3D image segmentation using micro-labor workforce. *Bioinformatics*, 29(10):1359–1360, 2013. 2

[13] D. Haehn, S. Knowles-Barley, M. Roberts, J. Beyer, N. Kasthuri, J. Lichtman, and H. Pfister. Design and evaluation of interactive proofreading tools for connectomics. *IEEE Transactions on Visualization and Computer Graphics (Proc. IEEE SciVis 2014)*, 20(12):2466–2475, 2014. 1, 2, 3, 5

[14] V. Jain, B. Bollmann, M. Richardson, D. Berger, M. Helmstädter, K. Briggman, W. Denk, J. Bowden, J. Mendenhall, W. Abraham, K. Harris, N. Kasthuri, K. Hayworth, R. Schalek, J. Tapia, J. Lichtman, and S. Seung. Boundary learning by optimization with topological constraints. In *Proc. IEEE CVPR 2010*, pages 2488–2495, 2010. 1, 2

[15] Janelia Farm. Raveler. https://openwiki.janelia.org/wiki/display/flyem/Raveler, 2014. Accessed on 31/03/2016. 1, 2

[16] A. Karimov, G. Mistelbauer, T. Auzinger, and S. Bruckner. Guided volume editing based on histogram dissimilarity. *Computer Graphics Forum*, 34(3):91–100, May 2015. 1, 3

[17] N. Kasthuri, K. J. Hayworth, D. R. Berger, R. L. Schalek, J. A. Conchello, S. Knowles-Barley, D. Lee, A. Vázquez-Reina, V. Kaynig, T. R. Jones, et al. Saturated reconstruction of a volume of neocortex. *Cell*, 162(3):648–661, 2015. 1, 4, 7

[18] V. Kaynig, T. Fuchs, and J. Buhmann. Neuron geometry extraction by perceptual grouping in sstem images. In *Proc. IEEE CVPR*, pages 2902–2909, 2010. 2

[19] V. Kaynig, A. Vazquez-Reina, S. Knowles-Barley, M. Roberts, T. R. Jones, N. Kasthuri, E. Miller, J. Lichtman, and H. Pfister. Large-scale automatic reconstruction of neuronal processes from electron microscopy images. *Medical image analysis*, 22(1):77–88, 2015. 1

[20] S. Knowles-Barley, M. Roberts, N. Kasthuri, D. Lee, H. Pfister, and J. W. Lichtman. Mojo 2.0: Connectome annotation tool. *Frontiers in Neuroinformatics*, (60), 2013. 1

[21] K. Lee, A. Zlateski, A. Vishwanathan, and H. S. Seung. Recursive training of 2d-3d convolutional networks for neuronal boundary detection. *arXiv preprint arXiv:1508.04843*, 2015. 2

[22] T. Liu, C. Jones, M. Seyedhosseini, and T. Tasdizen. A modular hierarchical approach to 3D electron microscopy image segmentation. *Journal of Neuroscience Methods*, 226(0):88 – 102, 2014. 1, 2

[23] J. Masci, A. Giusti, D. C. Ciresan, G. Fricout, and J. Schmidhuber. A fast learning algorithm for image segmentation with max-pooling convolutional networks. In *ICIP*, 2013. 1

[24] J. Nunez-Iglesias, R. Kennedy, T. Parag, J. Shi, and D. B. Chklovskii. Machine learning of hierarchical clustering to

segment 2D and 3D images. *PLoS ONE*, 8(8):e71715+, 2013. 2

[25] J. Nunez-Iglesias, R. Kennedy, S. M. Plaza, A. Chakraborty, and W. T. Katz. Graph-based active learning of agglomeration (GALA): A python library to segment 2D and 3D neuroimages. *Frontiers in Neuroinformatics*, 8(34), 2014. 1, 2

[26] H. Peng, F. Long, T. Zhao, and E. Myers. Proof-editing is the bottleneck of 3D neuron reconstruction: The problem and solutions. *Neuroinformatics*, 9(2-3):103–105, 2011. 2

[27] S. M. Plaza. Focused Proofreading: Efficiently Extracting Connectomes from Segmented EM Images, Sept. 2014. 2

[28] O. Ronneberger, P. Fischer, and T. Brox. U-net: Convolutional networks for biomedical image segmentation. *CoRR*, abs/1505.04597, 2015. 2

[29] S. Saalfeld, A. Cardona, V. Hartenstein, and P. Tomančák. CATMAID: collaborative annotation toolkit for massive amounts of image data. *Bioinformatics*, 25(15):1984–1986, 2009. 2

[30] S. Saalfeld, A. Cardona, V. Hartenstein, and P. Tomančák. As-rigid-as-possible mosaicking and serial section registration of large ssTEM datasets. *Bioinformatics*, 26(12):i57–i63, 2010. 2

[31] R. Sicat, M. Hadwiger, and N. J. Mitra. Graph abstraction for simplified proofreading of slice-based volume segmentation. In *EUROGRAPHICS Short Paper*, 2013. 1, 2

[32] M. G. Uzunbas, C. Chen, and D. Metaxas. An efficient conditional random field approach for automatic and interactive neuron segmentation. *Medical Image Analysis*, 27:31 – 44, 2016. Discrete Graphical Models in Biomedical Image Analysis. 1, 3

[33] A. Vázquez-Reina, M. Gelbart, D. Huang, J. Lichtman, E. Miller, and H. Pfister. Segmentation fusion for connectomics. In *Proc. IEEE ICCV*, pages 177–184, Nov 2011. 2